*Free Radical Research*, March 2011; 45(3): 276–292

informa
healthcare

# DCPIP (2,6-dichlorophenolindophenol) as a genotype-directed redox chemotherapeutic targeting NQO1*2 breast carcinoma

CHRISTOPHER M. CABELLO, SARAH D. LAMORE, WARNER B. BAIR III, ANGELA L. DAVIS, SARA M. AZIMIAN & GEORG T. WONDRAK

*Department of Pharmacology and Toxicology, College of Pharmacy, Arizona Cancer Center, University of Arizona, Tucson, AZ, USA*

*(Received date: 22 July 2010; In revised form date: 18 September 2010)*



**Abstract**

Accumulative experimental evidence suggests feasibility of chemotherapeutic intervention targeting human cancer cells by pharmacological modulation of cellular oxidative stress. Current efforts aim at personalization of redox chemotherapy through identification of predictive tumour genotypes and redox biomarkers. Based on earlier research demonstrating that anti-melanoma activity of the pro-oxidant 2,6-dichlorophenolindophenol (DCPIP) is antagonized by cellular NAD(P)H:quinone oxidoreductase (NQO1) expression, this study tested DCPIP as a genotype-directed redox chemotherapeutic targeting homozygous NQO1*2 breast carcinoma, a common missense genotype [rs1800566 polymorphism; NP_000894.1:p.Pro187Ser] encoding a functionally impaired NQO1 protein. In a panel of cultured breast carcinoma cell lines and NQO1-transfectants with differential NQO1 expression levels, homozygous NQO1*2 MDA-MB231 cells were hypersensitive to DCPIP-induced caspase-independent cell death that occurred after early onset of oxidative stress with glutathione depletion and loss of genomic integrity. Array analysis revealed upregulated expression of oxidative (*GSTM3*, *HMOX1*, *EGR1*), heat shock (*HSPA6*, *HSPA1A*, *CRYAB*) and genotoxic stress response (*GADD45A*, *CDKN1A*) genes confirmed by immunoblot detection of HO-1, Hsp70, Hsp70B', p21 and phospho-p53 (Ser15). In a murine xenograft model of human homozygous NQO1*2-breast carcinoma, systemic administration of DCPIP displayed significant anti-tumour activity, suggesting feasibility of redox chemotherapeutic intervention targeting the NQO1*2 genotype.

**Keywords:** *Redox chemotherapy, 2,6-dichlorophenolindophenol, xenograft, breast carcinoma, MDA-MB231, NQO1*2 genotype*

**Abbreviations:** *3-ABA, 3-aminobenzamide; AV, annexinV; b.i.d., bis in die/twice a day; DC, dicoumarol; DCFH-DA, 2',7'-dichlorodihydrofluorescein diacetate; DCPIP, 2,6-dichlorophenolindophenol; EGR1, early growth response gene 1; FITC, fluorescein isothiocyanate; GADD45A, growth arrest and DNA-damage-inducible alpha; GSH, glutathione; Hsp, heat shock protein; HO-1, heme oxygenase-1; NAC, $N^{\alpha}$-acetyl-L-cysteine; NQO1, NAD(P)H:quinone oxidoreductase 1; PARP, poly (ADP-ribose) polymerase; PI, propidium iodide; PIP, phenolindophenol; ROS, reactive oxygen species; SDS-PAGE, sodium dodecylsulphate polyacrylamide gel electrophoresis; TCEP, tris(2-carboxyethyl)phosphine.*

## Introduction

Accumulating experimental evidence suggests feasibility of chemotherapeutic intervention targeting human cancer cells through pharmacological modulation of cellular oxidative stress [1–4]. It has been suggested that differential redox set points in cancer cells vs non-transformed normal cells represent a therapeutic window of sufficient width permitting redox intervention that selectively targets cancer cells with constitutively up-regulated levels of reactive oxygen species (ROS) [1,5,6]. Much attention has therefore focused on the identification and development of experimental chemotherapeutics that induce positive deviations from redox homeostasis through

Correspondence: Georg T. Wondrak, PhD, University of Arizona, Arizona Cancer Center, 1515 North Campbell Avenue, Tucson, AZ 85724, USA. Tel: 520-626-9017. Fax: 520-626-3797. Email: wondrak@pharmacy.arizona.edu

ISSN 1071-5762 print/ISSN 1029-2470 online © 2011 Informa UK, Ltd.
DOI: 10.3109/10715762.2010.526766

pro-oxidant action, either by direct production of oxidizing species or by modulation of specific cellular targets involved in redox homeostasis [4,7–11]. Numerous investigational redox chemotherapeutics that induce pro-oxidant alterations of ROS-dependent mitogenic and survival signalling have shown clinical efficacy in human patients and are now undergoing detailed testing in advanced clinical trials [4], including the glutathione depleting cyanoaziridine-derivative imexon [12], the nitrofuran-based free radical generator nifurtimox [13], the iron-activated endoperoxide artemisinin [14,15], the texaphyrin-based redox cycler motexafin gadolinium [16], the molybdenium-based SOD-antagonist ATN-224 [17], the organic arsenical darinaparsin [18] and the thiol-directed mixed disulphide thioredoxin inhibitor PX-12 [19].

The pleiotropic mechanism of action associated with many redox chemotherapeutics involving simultaneous modulation of multiple redox-sensitive cellular targets may potentially compromise therapeutic window and benefit achievable with these agents [4,20]. Recent studies suggest that careful patient selection based on detailed tumour redox pheno- and genotyping may guide the selection of specific drugs that target the redox Achilles heel of the individual tumour with more efficiency and current efforts therefore aim at personalization of redox chemotherapeutic intervention through identification of predictive tumour genotypes and redox biomarkers [4,17,21–23].

In earlier research, we have demonstrated the pre-clinical anti-melanoma efficacy of the 2,6-dichlorophenol-indophenol{2,6-dichloro-4-[(p-hydroxyphenyl)imino]-2,5-cyclohexadien-1-one sodium salt, DCPIP; CAS# 620-45-1}, a pro-oxidant redox chemotherapeutic that impaired tumour growth in a murine xenograft model of human metastatic melanoma [24]. Remarkably, this membrane-permeable dihalogenated 1,4-benzoquinoneimine-type pro-oxidant [$E'^{o}$ (DCPIP) = + 0.22 V (two electron reduction potential); log $p$ (octanol/water) = 0.13] displays drug-like properties that include chemical stability, systemic deliverability, membrane permeability and low systemic toxicity established earlier in mice ($LD_{50}$ = 180 mg/kg; intravenous administration) [24,25]. Melanoma cell death induced by DCPIP was associated with rapid induction of oxidative stress and glutathione depletion and further studies revealed that DCPIP-induced cytotoxicity occurred as a function of cellular NAD(P)H:quinone oxidoreductase (NQO1) expression levels. Indeed, melanoma cell lines displaying high levels of NQO1 specific enzymatic activity were resistant to DCPIP-induced cell death and pharmacological or genetic antagonism of NQO1 sensitized melanoma cells to DCPIP, suggesting that sensitivity to DCPIP chemotherapeutic intervention represents a chemical vulnerability of NQO1 deficient tumours. Pre-clinical follow-up research has recently documented the cytotoxic, anti-angiogenic and anti-inflammatory activity of free and nanoparticle-encapsulated DCPIP targeting HCT116 colon carcinoma cells [26].

In our search for a specific cancer cell genotype that would sensitize human tumours to DCPIP cytotoxicity we focused our attention on the NQO1*2 genotype in human breast carcinoma. The common missense genotype NQO1*2 [rs1800566 polymorphism; NP_000894.1:p.Pro187Ser] encodes a functionally impaired NQO1 protein, rapidly degraded via the ubiquitin proteasomal pathway, causing the complete or partial absence of NQO1 enzymatic activity from homozygous and heterozygous carrier cells, respectively [27–30]. The NQO1*2 genotype strongly predicts poor survival among women with breast cancer and survival after metastasis is reduced among NQO1*2 homozygotes suggesting an involvement of NQO1 deficiency in cancer progression and treatment resistance [29]. Importantly, response to the anthracycline tumour antibiotic epirubicin is impaired in homozygous NQO1*2 breast carcinoma cells (MDA-MB231) *in vitro* and no drugs are currently available that would enable molecularly targeted chemotherapy of this important breast carcinoma genotype [29,31]. Based on our earlier findings on NQO1-modulation of DCPIP cytotoxicity in metastatic melanoma cells, we tested feasibility of using DCPIP as a genotype-directed redox chemotherapeutic that targets homozygous NQO1*2 breast cancer cells *in vitro* and *in vivo*.

## Material and methods

### *Chemicals*

All chemicals were purchased from Sigma Chemical Co (St. Louis, MO). The cell-permeable pancaspase inhibitor Z-VAD-fmk was from Calbiochem-Novabiochem (San Diego, CA). The PARP inhibitor PJ-34 was from Enzo Life Sciences Inc. (Farmingdale, NY).

### *Breast carcinoma cell lines and transfectants*

Human MDA-MB231 breast adenocarcinoma cells, displaying the homozygous NQO1*2 genotype [29], were purchased from ATCC (Manassas, VA) cultured in MEM supplemented with 10% foetal bovine serum, 2 mM HEPES, 2 mM L-glutamine, gentamicin (50 μg/ml) and bovine insulin (6 ng/ml). MCF-7 breast carcinoma cells display the heterozygous NQO1 genotype [29] and cells with increased NQO1 activity have been generated previously by stable transfection of an expression vector containing the rat NQO1 cDNA under the control of the β-actin promotor and encoding for neomycin resistance

(neo$^r$) [30]. Control transfectants (MCF-7-neo2) and the NQO1 over-expressing clone (MCF-7 DT15) with up to 30-fold greater NQO1 specific activity were obtained as a kind gift from Dr M. Briehl, University of Arizona, maintained in DMEM containing 10% foetal bovine serum (FBS) and G418 (0.3 mg/mL) [32]. All cells were maintained at 37°C in 5% $CO_2$, 95% air in a humidified incubator (referred to as 'normoxia'). Cytotoxicity of test compounds was also assessed under hypoxic conditions (24 h pre-conditioning of cells at 1% $O_2$, 5% $CO_2$, followed by addition of compound and incubation for another 24 h under the same conditions) using an Invivo Hypoxia Workstation 400 with a Ruskin hypoxic gas mixer (Biotrace, Cincinnati, OH).

*Cell proliferation assay*

Cells were seeded at 10 000 cells/dish on 35 mm dishes. After 24 h, cells were treated with test compound. Cell number at the time of compound addition and 72 h later were determined using a Z2 Analyser (Beckman Coulter, Inc., Fullerton, CA). Proliferation was compared with cells that received mock treatment. The same methodology was used to establish $IC_{50}$ values (drug concentration that induces 50% inhibition of proliferation of treated cells within 72 h exposure ± SD, $n = 3$).

*Cell death analysis*

Viability and induction of cell death (early and late apoptosis/necrosis) were examined by annexin-V-FITC (AV)/propidium iodide (PI) dual staining of cells followed by flow cytometric analysis as published previously [32]. Cells (100 000) were seeded on 35 mm dishes and received drug treatment 24 h later. Cells were harvested at various time points after treatment and cell staining was performed using an apoptosis detection kit according to the manufacturer's specifications (APO-AF, Sigma, St. Louis, MO).

*Caspase-3 activation assay*

Treatment-induced caspase-3 activation was examined in MDA-MB231 cells using a cleaved/activated caspase-3 (asp 175) antibody (Alexa Fluor 488 conjugate, Cell Signaling, Danvers, MA) followed by flow cytometric analysis as published recently [32].

*Human stress and toxicity pathfinder$^{TM}$ RT$^2$ profiler™ PCR expression array*

After pharmacological exposure, total cellular RNA ($3 \times 10^6$ MDA-MB231 cells) was prepared according to a standard procedure using the RNeasy kit (Qiagen, Valencia, CA). Reverse transcription was performed using the RT$^2$ First Strand kit (Superarray, Frederick, MD) and 5 µg total RNA. The RT$^2$ Human Stress and Toxicity Pathfinder$^{TM}$ PCR Expression Array (SuperArray) profiling the expression of 84 stress-related genes was run using the following PCR conditions: 95°C for 10 min, followed by 40 cycles of 95°C for 15 s alternating with 60°C for 1 min (Applied Biosystems 7000 SDS). Gene-specific product was normalized to GAPDH and quantified using the comparative $(\Delta\Delta C_t)$ $C_t$ method as described in the ABI Prism 7000 sequence detection system user guide as published earlier [24,33]. Expression values were averaged across three independent array experiments and standard deviation was calculated for graphing.

*Heme oxygenase-1 (HO-1) immunoblot analysis*

Following a published procedure, one day before treatment, $2 \times 10^6$ cells were seeded in T-75 flasks [34]. Cell growth medium was replaced 24 h after seeding, followed by addition of test compounds 60 min after medium change. Cells were incubated for 24 h (37°C, 5% $CO_2$), then washed with PBS, lysed in 1× SDS-PAGE sample buffer (200 µl, 0.375 M Tris HCl pH 6.8, 50% glycerol, 10% SDS, 5% β-mercaptoethanol, 0.25% bromophenol blue) and heated (3 min, 95°C). Samples (10 µl, containing ~ 45 µg total protein as determined by the BCA assay) were separated by 15% SDS-PAGE followed by immediate transfer to nitrocellulose membranes (Optitran, Whatman, Piscataway, NJ). The membrane was blocked with 5% milk in 0.1% PBST for 1 h. Rabbit anti-HO-1 polyclonal antibody (Stressgen Bioreagents, Ann Arbor, MI) was used 1:5000 in 5% milk-PBST overnight at 4°C. The membrane was washed three times for 10 min in 0.1% PBST before adding HRP-conjugated goat anti-rabbit antibody (Jackson Immunological Research, West Grove, PA) at 1:10 000 dilution followed by visualization using enhanced chemiluminescence detection reagents. Equal protein loading was examined by α-actin-detection using a mouse anti-actin monoclonal antibody (Sigma) at 1:1500 dilution.

*Immunoblot analysis of HSP70, HSP70', p53, phospho-p53 (Ser15), p21 (Waf1/Cip1) and PARP-1*

Sample preparation, SDS-PAGE, transfer to nitrocellulose and development occurred as described above. The following primary antibodies were used: rabbit anti-HSP70 polyclonal antibody (SPA-811; 1:1000) and mouse anti-HSP70B' monclonal antibody (SPA-754; 1: 1000; Assay Designs, Ann Arbor, MI); monoclonal mouse anti-p53 IgG (sc-71817; 1:1000) and polyclonal rabbit anti-phospho-p53 (Ser15) IgG (sc-101762; 1:1000; Santa Cruz Biotechnology, Santa Cruz, CA); mouse anti-p21 monoclonal antibody (1:2000) and monoclonal rabbit anti-PARP antibody

(1:1000; 46D11, Cell Signaling Technology, Danvers, MA) [33,35].

### *Measurement of NQO1-specific activity*

Determination of NQO1 specific activity was performed according to a published standard procedure [32]. In brief, cells ($2 \times 10^6$) were harvested by trysinization and resuspended in ice-cold TE (20 mM Tris-HCl with 2 mM EDTA, pH 7.4). Cells were disrupted in three cycles of freeze/thawing using liquid nitrogen and a 37°C waterbath, followed by centrifugation (12 000 g, 5 min). Protein concentration in the supernatant was determined using the BCA assay (Pierce, Rockford, IL). For determination of NQO1 specific activity the reaction mixture (1 ml final volume) contained 25 mM Tris-HCl (pH 7.4), 180 μM NADPH, BSA (0.2 mg/ml), Tween 20 [0.01 % (v/v)] and cell lysate (5 μl). The reaction was started by the addition of 2 μl 2,6-dichlorophenolindophenol (DCPIP, 20 mM stock in DMSO). Reduction of DCPIP was measured at room temperature for 1 min at 600 nm ($\varepsilon = 21 \times 10^3$ $M^{-1}cm^{-1}$) with or without 20 μM dicoumarol. The dicoumarol-inhibitable part of DCPIP reduction was used to calculate NQO1 activity expressed as nmol DCPIP × $(\text{mg protein})^{-1} \times \text{min}^{-1}$. A minimum of triplicate cultures were assayed.

### *Detection of intracellular oxidative stress by flow cytometric analysis*

Induction of intracellular oxidative stress by DCPIP was analysed by flow cytometry using 2',7'-dichlorodihydrofluorescein diacetate (DCFH-DA) as a sensitive non-fluorescent precursor dye according to a published standard procedure [32].

### *Assessment of oxygen consumption using an oxygen electrode*

Oxygen consumption by ascorbate-driven redox cycling of test quinones was examined following a published standard procedure using a Clark electrode (Oxygraph Plus, Hansatech Instruments, Norfolk, UK) [36]. The well-oxygenated reaction mixture (1 ml total volume, pH 7, 37°C) contained ascorbate (2 mM) in phosphate buffer (50 mM). The reaction was initiated by addition of menadione (20 μM) or DCPIP (up to 50 μM) with continuous magnetic stirring. Data recording and analysis were performed using the Oxygraph Plus software.

### *Determination of reduced and total cellular glutathione content*

Intracellular reduced glutathione was measured using the GSH-Glo Glutathione assay kit (Promega; San Luis Obispo, CA). Cells were seeded at 100 000 cells/dish on 35 mm dishes. After 24 h, cells were treated with test compound. At selected time points after addition of test compound, cells were harvested by trypsinization and then counted using a Coulter counter. Cells were washed in PBS and 10 000 cells/well (50 μl) were transferred onto a 96-well plate. A standard curve was prepared using a serial dilution of reduced glutathione. GSH-Glo reagent (50 μl) containing luciferin-NT and glutathione-S-transferase was then added followed by 30 min incubation. After addition of luciferin detection reagent to each well (100 μl) and 15 min incubation luminescence reading was performed using a BioTek Synergy 2 Reader (BioTek, Winooski, VT). For determination of total glutathione, sample treatment by *tris*(2-carboxyethyl) phosphine (TCEP, 1 mM final concentrations; 15 min incubation before addition of GSH-Glo reagent) leading to reductive regeneration of glutathione from protein-bound and other disulphide forms was performed. Data are normalized to GSH content in untreated cells and expressed as means ± SD ($n = 3$).

### *Mitochondrial transmembrane potential*

Mitochondrial transmembrane potential ($\Delta\psi m$) was assessed using the potentiometric dye 5,5',6,6'-tetrachloro-1,1',3,3'-tetraethylbenzimidazolylcarbocyanine iodide (JC-1) following a published procedure [37]. In brief, cells were trypsinized, washed in PBS, resuspended in 300 μl PBS containing 5 μg/ml JC-1 for 15 min at 37°C and 5% $CO_2$ in the dark, then washed twice in PBS and resuspended in 300 μl PBS. Bivariate analysis was performed by flow cytometry with excitation at 488 nm and mitochondrial function was assessed as JC-1 green (depolarized mitochondria, detector FL-1) or red (polarized mitochondria, detector FL-2) fluorescence.

### *Cell Glo ATP assay*

Cells were seeded at 50 000 cells/dish on 35 mm dishes. After 24 h, cells were treated with test compound. At various time points cells were counted and ATP content per 10 000 cells was determined using the CellTiter-Glo luminescent assay (Promega, Madison, WI) according to the manufacturer's instructions as published earlier [33]. Data are normalized to ATP content in untreated cells (expressed as means ± SD ($n = 3$).

### *Comet assay (alkaline single cell electrophoresis)*

The alkaline COMET assay was performed on MDA-MB231 cells according to the manufacturer's instructions (Trevigen, Gaithersburg, MD) as published recently [35]. After treatment, cells (100 000 per

100 mm dish) were harvested by gently scraping and suspended in 500 µl DPBS. An aliquot (50 µl) was mixed with low-melting-point agarose (450 µl) and spread on pre-treated microscope slides. To allow DNA unwinding and expression of alkali-labile sites, slides were exposed to alkaline buffer (1 mM EDTA and 300 mM NaOH, pH > 13) protected from light at room temperature for 45 min. Electrophoresis was conducted in the same alkaline buffer for 20 min at 300 mA. After electrophoresis, slides were rinsed three times in distilled $H_2O$, then fixed in 70% ethanol for 5 min. Cells were stained with SYBR™ Green and then visualized and analysed using a fluorescence microscope (fluorescein filter) and CASP software. At least 75 tail moments for each group were analysed in order to calculate the mean ± SD for each group.

### *siRNA transfection targeting PARP-1 expression*

MDA-MB231 cells were transiently transfected with a 100 nmol pool of four small interfering RNA (siRNA) oligonucleotides (oligos) targeting PARP1 or a 100 nmol pool of four non-targeting siRNA oligos using the DharmaFECT 1 transfection reagent (Dharmacon RNA Technologies, Lafayette, CO) following a standard procedure [24]. The sequences of siGENOME PARP1 SMARTpool (PARP1 siRNA) (GenBank: NM 001618) were GAAAGUGUGUUCAACUAAU; GCAACAAACUGGAACAGAU; GAAGUCAUCGA UAUCUUUA; and GAUAGAGCGUGAAGGCGAA. The oligos were resuspended in the Dharmacon 1x siRNA buffer and incubated in serum-free media for 5 min. The oligos were incubated with the transfection reagent for 20 min before cellular treatment. Complete media was added to the siRNA oligo mixture and the cells were incubated with the siRNAs in appropriate cell culture conditions for 48 h. Cells were then re-transfected with another 100 nmol pool of four siRNA oligonucleotides targeting PARP1 or a 100 nmol pool of four non-targeting siRNA oligonucleotides. After another 24 h, cells were either harvested for confirmation of PARP-1 knockdown by immunoblot blot analysis or exposed to DCPIP followed by viability assessment using flow cytometric analysis of AV-FITC/PI stained cells.

### *Human NQO1*2 breast carcinoma SCID mouse xenograft model*

All procedures were completed in accordance with the University of Arizona Institutional Animal Care and Use Committee (IACUC) protocol (# 07-029, approved 24 May 2007). MDA-MB231 human adenocarcinoma cells (> 90% viability) were resuspended at the concentration of 10 × 106 cells/100 µl of sterile saline. A SCID mouse colony was developed at the University of Arizona using original SCID (C.B-17/IcrACCSCID) obtained from Taconic (Germantown, NY). MDA-MB231 cells ($10 \times 10^6$ cells in matrigel, 0.1 ml injection volume) were injected subcutaneously into the lower left mammary fat pad of female SCID mice (day 0) and after tumours became established (~ 100 $mm^3$; day 30) mice were pair-matched into the treatment groups. The following day, treatment with drug in PBS or PBS only was initiated. The chemotherapeutic test agent DCPIP (1 mg per ml PBS) was prepared and administered by intraperitoneal injection in less than 1 h. DCPIP ($10\ mg \times kg^{-1} \times d^{-1}$, 100 µl, b.i.d., $n = 10$) was given on days 1–6 and 8–14 post the day of pair-matching, whereas control animals received carrier only (PBS, $n = 12$). Subcutaneous tumours were measured twice weekly for tumour volume estimation ($mm^3$) in accordance with the formula $(a^2 \times b)/2$, where $a$ is the smallest diameter and $b$ is the largest diameter. The mice were sacrificed individually by $CO_2$ when the tumours reached a volume of 2000 $mm^3$. Tumour growth curves were obtained by determining average tumour volumes until day 70 after cell injection and data points were analysed using the two-sided Student's $t$-test ($^*p < 0.05$; $^{**}p < 0.01$; $^{***}p < 0.001$).

### *Immunohistochemical characterization of tumour tissue from mice xenografts*

At the end of the experiment, tumours from SCID mice were harvested and tumour tissue sections were analysed for expression of p21. Confirmatory murine experimentation was performed by Applied Xenomics, Inc (Basel, Switzerland). Briefly, tissues were harvested, fixed in 10% neutral buffered formalin for 24 h, processed and embedded in paraffin. Routine haematoxylin stain was performed on three micron sections of tissue and immunohistochemistry was performed using a mouse monoclonal antibody to p21 (DCS60; Cell Signaling Technology; 1:100 dilution). Detection of primary antibody was performed on a Discovery XT Automated Immunostainer (Ventana Medical Systems, Inc, Tucson, AZ) using a biotinylated-streptavidin-HRP and DAB system. Haematoxylin counterstaining was also performed online. Following staining on the instrument, slides were dehydrated through graded alcohols to xylene and coverslipped with Pro-Texx mounting medium. Images were captured using an Olympus BX50 and Spot (Model 2.3.0) camera. Images were standardized for light intensity. No automated analysis of the data was performed.

### *Statistical analysis*

Unless indicated differently, the results are presented as means ± SD of at least three independent experiments. They were analysed using the two-sided Student's $t$-test ($^*p < 0.05$; $^{**}p < 0.01$; $^{***}p < 0.001$).

## Results

### *NQO1*2 MDA-MB231 breast carcinoma cells are hypersensitive to DCPIP-induced caspase-independent cell death*

Our earlier experiments in cultured melanoma cell lines have demonstrated that the expression level of enzymatically active NQO1 represents a crucial determinant of DCPIP cytotoxicity [24]. We therefore tested the hypothesis that the homozygous NQO1*2 genotype of MDA-MB231 breast carcinoma cells, characterized by complete absence of NQO1 specific enzymatic activity, confers high sensitivity to DCPIP-induced cytotoxicity. To this end, DCPIP cytotoxicity was examined in a focused panel of cultured human breast carcinoma cell lines with documented differential NQO1 expression levels as assessed earlier in our laboratory (numbers indicate specific enzymatic activity as nmol reduced DCPIP $\times$ (mg cellular protein)$^{-1}$ $\times$ min$^{-1}$ [29,30,32]): (I) MDA-MB231 displaying the homozygous NQO1*2 genotype with complete absence of NQO1 enzymatic activity from cytosolic extracts (specific enzymatic activity: not detectable); (II) NQO1-heterozygous MCF7 cells (only one wildtype NQO1*1 allele) expressing moderate levels of endogenous, enzymatically active NQO1 protein, stably transfected with a control vector (MCF7-neo2; specific enzymatic activity: 370 $\pm$ 40); and (III) NQO1-heterozygous MCF7 cells (only one wildtype NQO1*1 allele), stably transfected with a rat NQO1-encoding expression vector leading to massive up-regulation of enzymatically active NQO1 protein levels (MCF7-DT15; specific enzymatic activity: 8600 $\pm$ 300). First, the dose-response of DCPIP cytotoxicity was examined by flow cytometric analysis of breast carcinoma cell viability (Figure 1). Indeed, exposure to low micromolar concentrations of DCPIP (24 h, $LD_{50}$ = 23.0 $\pm$ 3.4 μM; Figures 1A and E) induced MDA-MB231 cell death that was not associated with proteolytic activation of caspase 3 (Figure 1B) and could not be blocked by co-treatment with the pancaspase inhibitor zVADfmk (Figure 1C). These data are consistent with a caspase-independent mode of cell death activated by DCPIP in this NQO1-disabled cell line.

Next, we observed that viability of NQO1 over-expressing MCF-7-DT15 was maintained even upon exposure to very high concentrations of DCPIP (Figures 1D and E; $LD_{50}$ >> 80 μM; data not shown). For example, at 40 μM DCPIP, viability was strongly reduced in MDA-MB231 cells (14.2 $\pm$ 8.6% viable cells; Figures 1A and E), but was not impaired significantly in MCF7-DT15 cells (87.4 $\pm$ 3.9 % viable cells; Figures 1D and E). MCF7-neo2 cells with moderate endogenous NQO1 specific enzymatic activity displayed intermediate-level DCPIP-sensitivity (Figures 1D and E; $LD_{50}$ = 63.5 $\pm$ 5.5 μM). A similar sensitivity differential that correlates with expression levels of enzymatically active NQO1 was observed when potency of inhibition of proliferation by DCPIP was assessed. Again, MDA-MB231 were highly sensitive ($IC_{50}$ = 1.8 $\pm$ 0.5 μM), whereas MCF7-DT15 displayed high resistance ($IC_{50}$ = 41.8 $\pm$ 4.7 μM), and MCF7-neo2 displayed intermediate sensitivity ($IC_{50}$ = 13.5 $\pm$ 3.7 μM) (72 h continuous exposure, data not shown).

### *Stress response gene expression and p53-Ser15 phosphorylation are activated in DCPIP-exposed MDA-MB231 breast carcinoma cells*

Modulation of stress and toxicity response gene expression was examined in MDA-MB231 cells exposed to DCPIP (20 μM, 24 h exposure) using the RT$^2$ Human Stress and Toxicity Profiler$^{TM}$ PCR Expression Array technology (SuperArray, Frederick, MD) (Figure 2A). Out of 84 stress-related genes contained on the array DCPIP-induced expression changes in MDA-MB231 cells affected 18 genes by at least 5-fold over untreated control cells, as summarized in Figure 2A (table, right panel). Genes that were more than 10-fold up-regulated encoded the oxidative stress responsive *heat shock proteins Hsp70B'* (HSPA6; 4285-fold), *Hsp70* (HSPA1A; 73-fold) and *alpha-crystallin B chain* (CRYAB; 18-fold) [38], the electrophilic stress response enzymes glutathione S-transferase M3 (GSTM3; 57-fold) and *heme oxygenase-1* (HMOX1; 17-fold) and the oxidative stress-responsive transcription factor and tumour suppressor *early growth response protein 1* (EGR1; 14-fold) [39]. In addition, genes encoding the apoptogenic and inflammatory cytokines *tumour necrosis factor-alpha* (TNF; 122-fold) and the tumour necrosis factor family member *lymphotoxin alpha* (LTA; 13-fold) were up-regulated significantly. With particular significance in the context of anti-proliferative and genotoxic stress response, genes encoding the p53-regulated anti-proliferative *cyclin-dependent kinase inhibitor 1* (*p21, Waf1/Cip1*) (CDKN1A; 20-fold) and *growth arrest and DNA-damage-inducible, alpha* (GADD45A; 6-fold) were strongly up-regulated in response to DCPIP exposure [40–42].

Next, DCPIP-induced up-regulation of cellular HMOX1, HSPA6, HSPA1A and CDKN1A gene expression was examined at the protein level by immunoblot analysis (Figures 2B–G). Generally, DCPIP-induced gene expression changes assessed at the protein level were not always dose-dependent, consistent with the hypothesis that at higher doses of DCPIP general cytotoxicity compromises cellular protein biosynthesis. For example, up-regulation of HO-1 protein (encoded by HMOX1) in response to 10 μM DCPIP was more pronounced than in response to 20 μM DCPIP (Figures 2B and C). Up-regulation of cellular HO-1 protein levels was detected within

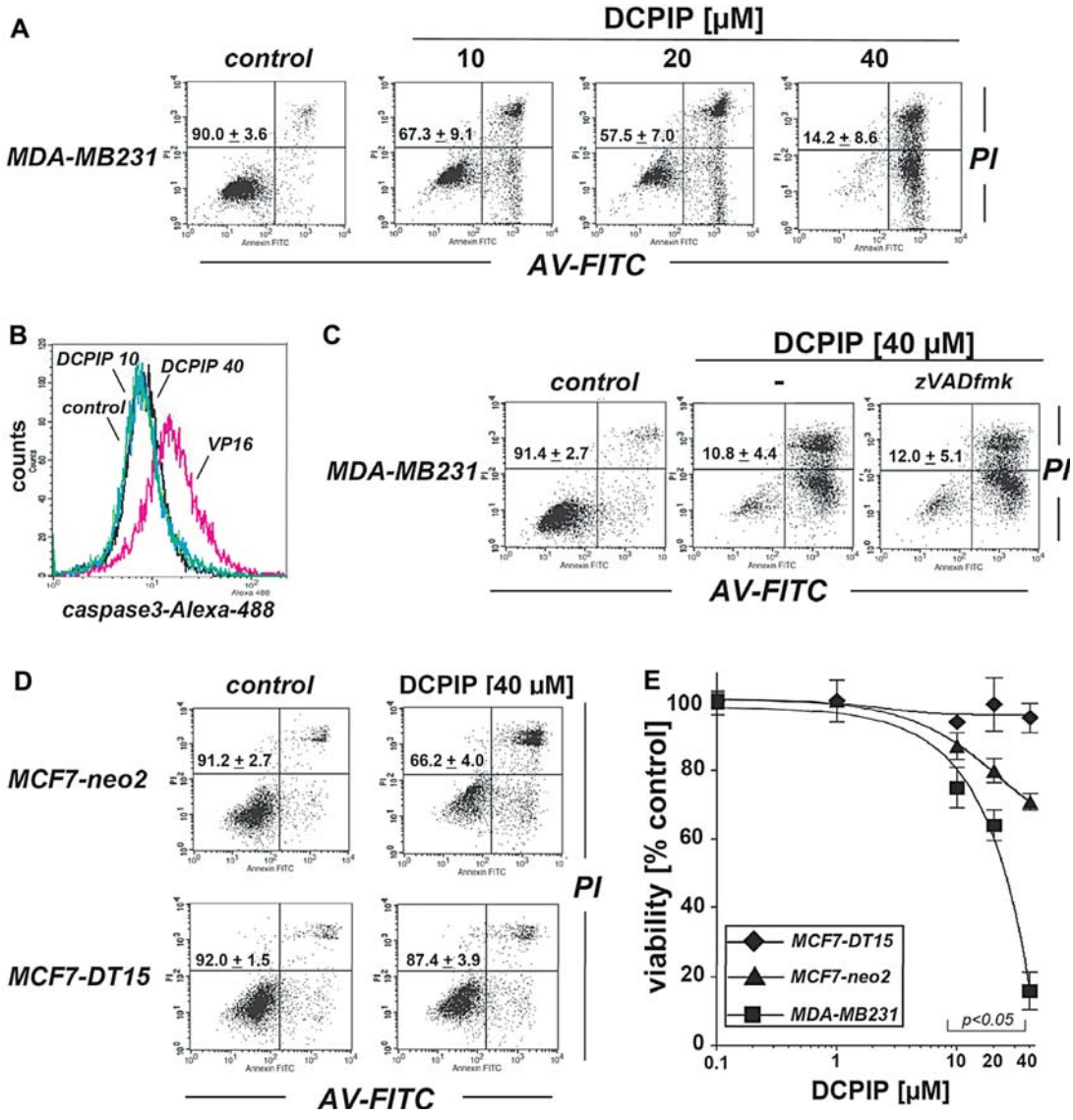


Figure 1. MDA-MB231 breast carcinoma cells are hypersensitive to DCPIP-induced caspase-independent cell death. (A) Induction of MDA-MB231 cell death by exposure to increasing doses of DCPIP (up to 40 μM, 24 h) as assessed by flow cytometric analysis of annexinV-FITC/propidium iodide (AV/PI)-stained cells. The numbers indicate viable cells ($AV^-$, $PI^-$, lower left quadrant) in percentage of total gated cells (mean ± SD, $n = 3$). (B) DCPIP-induced (10 and 40 μM, 24 h) caspase-3 activation as examined by flow cytometric detection using an Alexa Fluor 488-conjugated monoclonal antibody against cleaved procaspase-3. Exposure to etoposide (VP16, 20 μM, 24 h) was used to generate a positive control. One representative experiment out of three similar repeats is shown. (C) Induction of MDA-MB231 cell death by exposure to DCPIP (40 μM, 24 h) in the absence or presence of the pancaspase inhibitor zVADfmk (40 μM, 1 h pre-incubation before addition of DCPIP) analysed as in (A). (D) DCPIP-induced (40 μM, 24 h) death of NQO1-over-expressing MCF7 breast carcinoma transfectants (MCF7-DT15) and vector control transfected cells (MCF7-neo) analysed as in (A). (E) Comparative dose–response relationship of DCPIP-induced cell death in MDA-MB231, MCF7-DT15 and MCF7-neo2 breast carcinoma cells as assessed by AV/PI flow cytometry (mean ± SD, $n = 3$; $p < 0.05$ for [DCPIP] ≥ 10 μM (MDA-MB231 vs MCF7-neo2)).

6 h exposure to DCPIP. Protein levels of Hsp70B' (encoded by HSPA6) and Hsp70 (encoded by HSPA1A) were also strongly up-regulated within 12 h exposure to DCPIP (10 μM) (Figure 2D). Significant up-regulation of cellular protein levels of p21, the CDKN1A gene product, occurred in response to DCPIP treatment and was detectable within 3 h exposure time (Figures 2E and F). DNA damage is known to induce activational phosphorylation of tumour suppressor protein p53 at Ser15 that occurs by genotoxic stress-responsive kinases [43]. Consistent with an involvement of p53 activation that may occur upstream or independent of p21 up-regulation [42], early activational phosphorylation of p53, assessed by immunoblot analysis of phospho-p53 (Ser15) vs total p53 protein levels, was observed in response to DCPIP within 3 h exposure time (Figure 2G). However, at concentrations ≤ 1 μM, treatment with DCPIP was not associated with cytotoxicity (loss of viability) and no changes in protein expression or phosphorylation status were observed (data not shown).

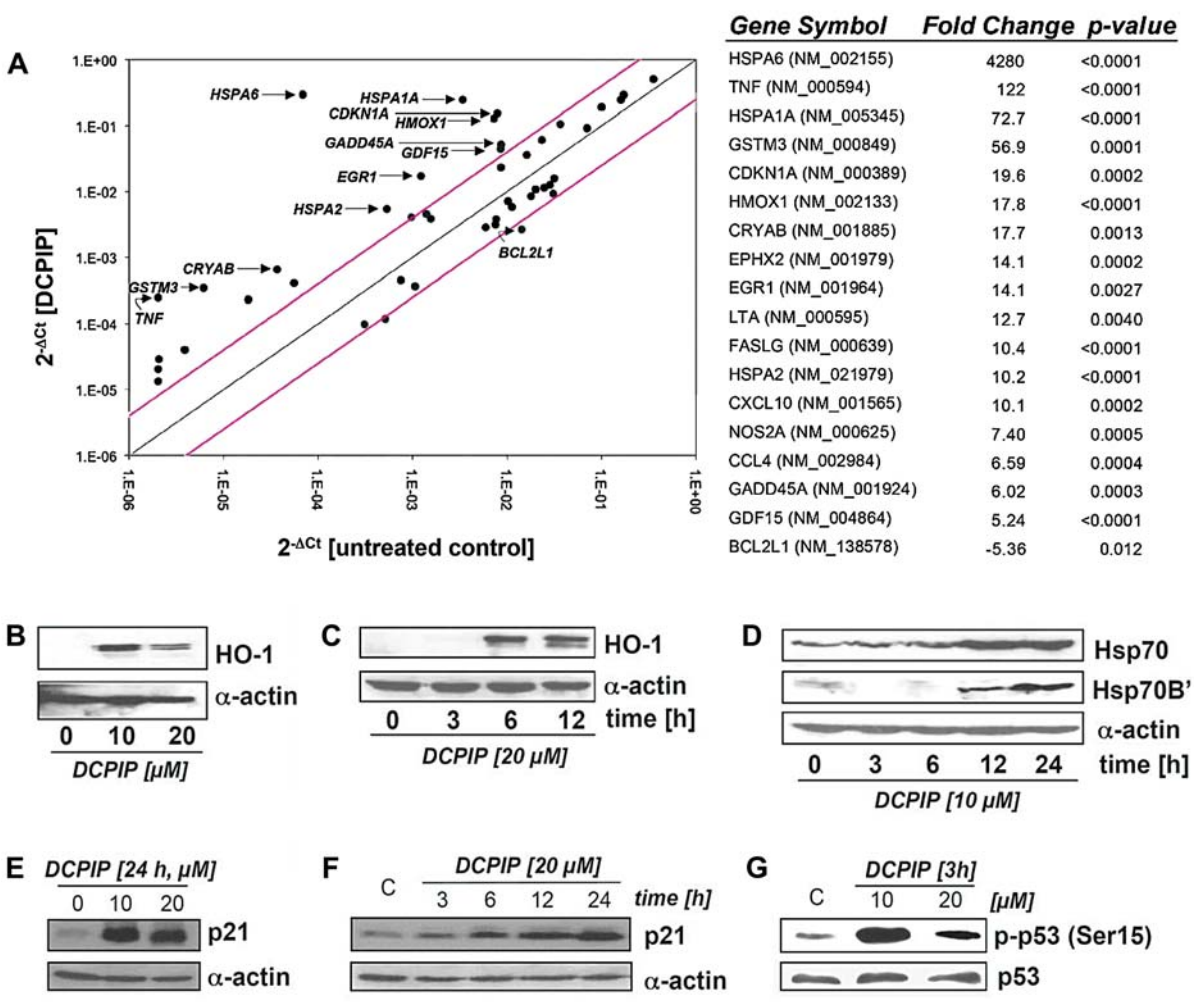


| Gene Symbol | Fold Change | p-value |
|---|---|---|
| HSPA6 (NM_002155) | 4280 | <0.0001 |
| TNF (NM_000594) | 122 | <0.0001 |
| HSPA1A (NM_005345) | 72.7 | <0.0001 |
| GSTM3 (NM_000849) | 56.9 | 0.0001 |
| CDKN1A (NM_000389) | 19.6 | 0.0002 |
| HMOX1 (NM_002133) | 17.8 | <0.0001 |
| CRYAB (NM_001885) | 17.7 | 0.0013 |
| EPHX2 (NM_001979) | 14.1 | 0.0002 |
| EGR1 (NM_001964) | 14.1 | 0.0027 |
| LTA (NM_000595) | 12.7 | 0.0040 |
| FASLG (NM_000639) | 10.4 | <0.0001 |
| HSPA2 (NM_021979) | 10.2 | <0.0001 |
| CXCL10 (NM_001565) | 10.1 | 0.0002 |
| NOS2A (NM_000625) | 7.40 | 0.0005 |
| CCL4 (NM_002984) | 6.59 | 0.0004 |
| GADD45A (NM_001924) | 6.02 | 0.0003 |
| GDF15 (NM_004864) | 5.24 | <0.0001 |
| BCL2L1 (NM_138578) | -5.36 | 0.012 |

Figure 2. DCPIP induces stress response gene expression and p53-Ser15 activational phosphorylation in MDA-MB231 breast carcinoma cells. (A) The scatter blot (left panel) depicts differential gene expression as detected by the RT$^2$ Human Stress and Toxicity Profiler$^{TM}$ PCR Expression Array technology profiling the expression of 84 (oxidative) stress- and toxicity-related genes after DCPIP treatment (20 μM, 24 h). Upper and lower lines represent the cut-off indicating 4-fold up- or down-regulated expression, respectively. Arrows specify selected genes with at least 4-fold up-regulated expression vs untreated controls. Expression array analysis was performed in three independent repeats and analysed using the two-sided Student's *t*-test. The table (right panel) summarizes statistically significant expression changes by at least 3-fold ($p < 0.05$). (B–G) Immunoblot detection of DCPIP-induced protein levels in MDA-MB231 cells: (B) Modulation of cellular heme oxygenase-1 (HO-1) protein levels by DCPIP (10 and 20 μM, 24 h) as examined by immunoblot analysis of total cellular protein extracts. Detection of α-actin expression served as a loading control. (C) Early time course of DCPIP-modulation (20 μM; 3–12 h) of HO-1 protein levels. (D) Time course of DCPIP-modulation (10 μM; 3–24 h) of Hsp70 and Hsp70B' protein levels. (E) DCPIP-modulation (10 and 20 μM, 24 h) of cellular p21 protein levels. (F) Time course of DCPIP-modulation (20 μM; 3–24 h) of p21 protein levels. (G) Early activational phosphorylation of p53 as assessed by immunoblot analysis of p-p53 (Ser15) and total p53 protein levels (DCPIP 10–20 μM; 3 h exposure).

### *Early induction of oxidative stress and depletion of cellular ATP levels occur in DCPIP-treated MDA-MB231 breast carcinoma cells*

Consistent with earlier observations on DCPIP-induced cytotoxicity and oxidative stress in human melanoma cell lines [24], up-regulation of cellular oxidative stress in response to DCPIP exposure (20 μM, 1 and 6 h exposure time) was examined by flow cytometric determination of 2',7'-dichlorodihydrofluorescein diacetate (DCFH-DA) oxidation (Figure 3A). Indeed, mean intensity of cellular DCF-fluorescence increased by ~ 8-fold within 1 h of DCPIP-exposure, indicative of massive pro-oxidant deviations from cellular redox homeostasis at this early time point. As an additional sensitive marker of cellular stress induced by DCPIP, energy depletion was assessed by determination of cellular ATP levels reaching the level of statistical significance after 6 h exposure (DCPIP 20 μM; Figure 3B). Consistent with early mitochondrial impairment that might be mechanistically linked to DCPIP-dependent induction of oxidative stress (Figure 3A) and depletion of cellular ATP levels (Figure 3B), loss of mitochondrial transmembrane potential ($\Delta\psi m$) could be detected by

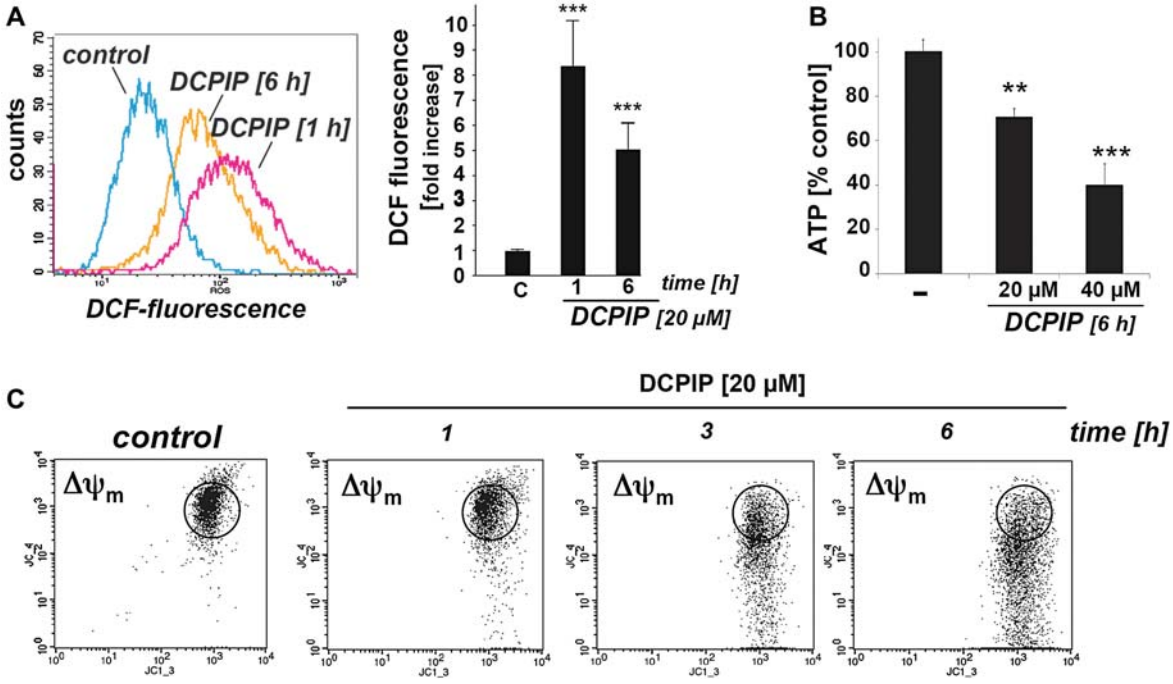


Figure 3. DCPIP induces oxidative stress and energy crisis in MDA-MB231 breast carcinoma cells. (A) Induction of cellular oxidative stress was assessed by flow cytometric determination of 2',7'-dichlorodihydrofluorescein diacetate (DCFH-DA) oxidation in response to DCPIP exposure (20 μM, 1 and 6 h exposure time). Histograms depict one representative experiment (left panel) and bar graph analysis represents three similar repeats (right panel; mean ± SD, $n = 3$). (B) Energy depletion in response to DCPIP (20 and 40 μM, 6 h) was assessed by determination of cellular ATP levels. (C) Time course analysis of loss of mitochondrial transmembrane potential (Δψm) in response to DCPIP exposure (20 μM; 1, 3 and 6 h) as assessed by flow cytometric analysis of JC-1 stained cells. One representative experiment of three similar repeats is shown.

flow cytometric analysis of JC-1 stained cells that were exposed to DCPIP (Figure 3C; 20 μM, 3 h exposure time). Importantly, these early molecular changes were detected in DCPIP-treated cells that did not yet display compromised plasma membrane integrity or reduced cell viability as assessed by flow cytometry (see Figure 4B).

### *MDA-MB231 breast carcinoma cells are hypersensitive to DCPIP-induced glutathione depletion*

In the context of rapid induction of oxidative stress by DCPIP, we then tested the hypothesis that MDA-MB231 breast carcinoma cells may display hypersensitivity to DCPIP-induced glutathione depletion. To this end, dose response (10–40 μM DCPIP) and time course (up to 6 h exposure time) of modulation of intracellular reduced glutathione content in MDA-MB231, MCF7-DT15 and MCF7-neo2 breast carcinoma cells was examined (Figure 4A). As observed in the comparative cytotoxicity study presented in Figure 1, DCPIP-induced glutathione depletion preferentially targeted MDA-MB231 cells where massive reduction of glutathione by almost 50% of untreated control levels was detectable within 30 min of exposure to DCPIP at concentrations as low as 10 μM (Figure 4A, left panel), long before cell viability and plasma membrane integrity were impaired (Figure 4B). Similar depletion of cellular glutathione was observed when cells were incubated in PBS containing DCPIP (30 min, 10–40 μM; data not shown), excluding the possibility that chemical reactions between medium or serum constituents and DCPIP are responsible for cellular glutathione depletion. In contrast to MDA-MB231 cells, NQO1 over-expressing MCF7-DT15 cells were resistant to DCPIP-induced glutathione depletion and only extended exposure (6 h) to higher concentrations (40 μM) induced a moderate reduction of cellular glutathione levels (Figure 4A, centre panel). MCF7-neo2 cells with low levels of endogenous NQO1 expression displayed an intermediate sensitivity to DCPIP-induced glutathione depletion (Figure 4A, right panel).

Consistent with a causative role of glutathione depletion in DCPIP-induced MDA-MB231 cell death, significant sensitization of DCPIP-induced cytotoxicity (20 μM, 24 h exposure) was observed in cells that were pre-exposed to the inhibitor of glutathione biosynthesis L-buthionine-S,R-sulphoximine (BSO, 1 mM; 24 h pre-incubation; Figure 4C) [24]. Conversely, MDA-MB231 cell viability was largely maintained after pre-incubation with the glutathione precursor N-acetyl-L-cysteine (NAC, 10 mM; 24 h pre-incubation) performed before DCPIP-exposure (40 μM; 24 h; Figure 4D).

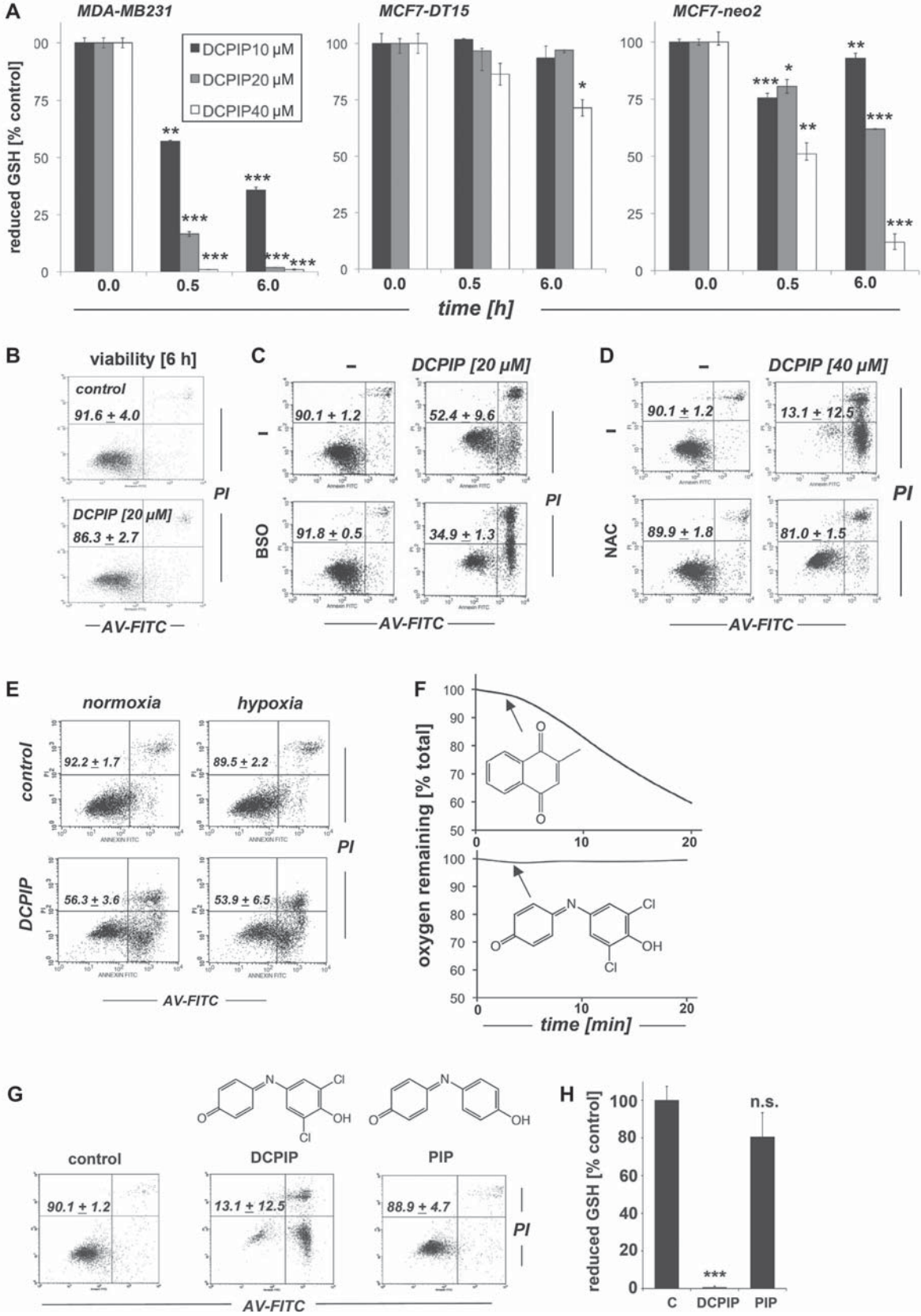


Figure 4. MDA-MB231 breast carcinoma cells are hypersensitive to DCPIP-induced early glutathione depletion. (A) Modulation of intracellular reduced glutathione content in MDA-MB231, MCF7-DT15 and MCF7-neo2 breast carcinoma cells exposed to DCPIP (10–40 µM, up to 6 h). Reduced glutathione content was determined as detailed in Materials and methods and normalized to cell number (mean ± SD, $n = 3$). (B–E) Viability of MDA-MB231 cells exposed to DCPIP was examined by flow cytometric analysis of AV/PI-stained cells as detailed in Figure 1A (mean ± SD, $n = 3$): (B) Viability of MDA-MB231 cells exposed to DCPIP (20 µM, 6 h). (C) Modulation of MDA-MB231 cell viability after pre-incubation (24 h) with BSO (1 mM) followed by DCPIP exposure (20 µM, 24 h). (D) Modulation

Next, potency of induction of MDA-MB231 cell death by DCPIP was examined as a function of oxygen availability using a regular cell culture incubator ('normoxia') and a hypoxic chamber (1% oxygen, 'hypoxia'). We observed that DCPIP-cytotoxicity (20 μM, 24 h) was not attenuated under hypoxic conditions (Figure 4E). Moreover, kinetics and extent of DCPIP-induced glutathione depletion, observed earlier under normoxic conditions (Figure 4A), were not changed significantly under hypoxic conditions (data not shown). These data indicate that oxygen availability is not a crucial determinant of DCPIP-induced cytotoxicity and glutathione depletion suggesting feasibility of using this agent for cancer cell elimination even under conditions of tumour hypoxia.

Further chemical experimentation using a Clark electrode examined the possibility that DCPIP can undergo ascorbate-driven redox cycling, an oxygen-dependent reactivity that has recently been shown to be causatively involved in pro-oxidant elimination of human leukaemia cells by the experimental anticancer quinone menadione [36]. Indeed, ascorbate-driven (2 mM) redox cycling of menadione (20 μM, pH 7) caused reductive oxygen consumption at an appreciable rate (complete reaction mixture: reduction of total oxygen content by 2.2% per min; ascorbate only: reduction of total oxygen content by 0.35% per min; Figure 4F, upper panel). However, no steady oxygen consumption was observed in an analogous reaction mixture containing ascorbate (2 mM) and DCPIP (up to 50 μM, pH 7; Figure 4F, lower panel). Taken together, these data demonstrate that DCPIP-induced glutathione depletion and cytotoxicity are maintained under hypoxic conditions (Figure 4E) and indicate the inability of DCPIP to undergo ascorbate-driven redox cycling (Figure 4F). These findings are consistent with a mechanism of action underlying glutathione depletion that does not require a molecular interaction between DCPIP and oxygen and may rather depend on covalent thiol-adduction, a chemical reaction based on Michael addition reported earlier in the context of DCPIP-glutathione reactions as discussed below [44].

Interestingly, depletion of cellular glutathione levels was not observed when the dechlorinated DCPIP-analogue 4-(4-hydroxyphenyl)iminocyclohexa-2,5-dien-1-one (phenolindophenol, PIP) was tested in MDA-MB231 cells (40 μM, each; 24 h exposure; Figures 4G and H). Absence of the two chlorine atoms from the 2- and 6-positions of the aromatic quinoneimine core completely abolished cytotoxic and glutathione-depleting activity of the test compound, suggesting a crucial role of these electronegative substituents in electrophilic activation and MDA-MB231-directed chemotherapeutic activity of DCPIP [24,45].

### *DCPIP induces genotoxic stress with rapid impairment of genomic integrity in MDA-MB231 breast carcinoma cells*

Our observation that DCPIP treatment caused genotoxic stress response gene expression (GADD45A and CDKN1A; Figure 2A) with rapid up-regulation of p21 protein levels (Figures 2E and F) and p53 (Ser15) activational phosphorylation (Figure 2G) lead us to examine the possibility that early induction of DNA damage may contribute to DCPIP-cytotoxicity in MDA-MB231 cells (Figure 5). Using alkaline single cell electrophoresis (comet assay) as a sensitive genotoxicity assay [35,46], the integrity of cellular DNA was examined in MDA-MB231 cells treated with DCPIP (20 μM, 30 min up to 6 h exposure time). In addition, cells were exposed to $H_2O_2$, an established genotoxic agent serving as a positive control. As evident from formation of nuclear comets, indicative of DNA unwinding under alkaline conditions resulting from single or double strand breaks, AP-site formation or nucleotide excision repair [46], significant induction of genotoxic stress was detectable within 30 min exposure to DCPIP (Figure 5A). DCPIP treatment induced comets with average tail moments that exceeded control levels ~ 6-fold within 6 h of exposure (Figure 5A, right panel). Again, it is important to note that DCPIP-induced DNA damage occurred in cells without compromised viability that was maintained over at least 6 h continuous exposure to 20 μM DCPIP (Figure 4B).

Earlier research has demonstrated that DNA damage-dependent activation of poly(ADP-ribose) polymerase (PARP-1) may cause rapid depletion of cellular ATP levels with induction of caspase-independent cell death in response to genotoxic agents including hydrogen peroxide and quinone-based pro-oxidants [35,47]. We therefore tested the hypothesis that PARP-1 activation is causatively involved in DCPIP-induced ATP depletion and MDA-MB231 cell death (Figures 5B and C). However, DCPIP-induced ATP depletion was not antagonized by co-treatment with PARP-1 inhibitors 3-aminobenzamide

of MDA-MB231 cell viability after pre-incubation (24 h) with NAC (10 mM) followed by DCPIP exposure (40 μM, 24 h). (E) Viability of MDA-MB231 cells exposed to DCPIP (20 μM, 24 h) under normoxic (5% oxygen) or hypoxic (1% oxygen) conditions analysed by flow cytometry. (F) Ascorbate-driven (2 mM) redox cycling of menadione (20 μM, upper panel) or DCPIP (50 μM, lower panel) was assessed measuring oxygen consumption using a Clark electrode (pH 7, 50 mM oxygenated phosphate buffer, 37°C). Arrows indicate time point of addition of the respective quinone compound to the complete assay mixture. (G) Comparative cytotoxicity of DCPIP and PIP (40 μM, each; 24 h exposure) in MDA-MB231 cells. (H) Modulation of intracellular reduced glutathione content by DCPIP and PIP exposure (40 μM, 6h) as detailed in (A).

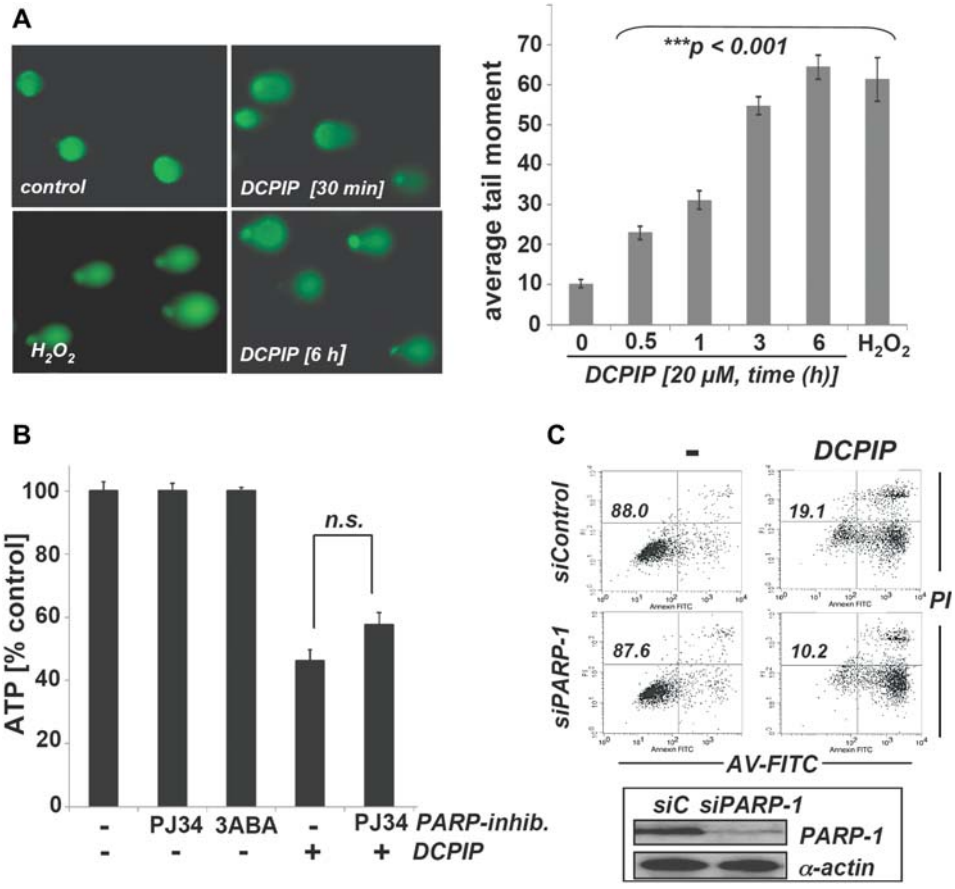


Figure 5. DCPIP induces genotoxic stress with early impairment of genomic integrity in human MDA-MB231 breast carcinoma cells. (A) Cells were exposed to DCPIP (20 μM, 0.5–6 h) and DNA damage was detected using the comet assay as described in Materials and methods. As a positive control cells were exposed to $H_2O_2$ (100 μM, 30 min). Representative comet images (left panel) as visualized by fluorescence microscopy and quantitative analysis of average tail moments (right panel) are shown. (B) DCPIP-induced ATP depletion as a function of PARP inhibition. Cells were exposed to DCPIP (20 μM, 6 h) after 1 h pre-exposure to the pharmacological PARP-1 inhibitors 3-ABA (4 mM) and PJ34 (1 μM). (C) Genetic down-regulation of PARP-1 expression does not confer protection of MDA-MB231 cells against DCPIP-induced cytotoxicity. Induction of cell death by exposure to DCPIP (40 μM, 24 h) was examined using AV/PI flow cytometric analysis of MDA-MB231 cells after control siRNA treatment (siControl, siC) and PARP-1 siRNA knockdown (siPARP-1). The numbers indicate viable cells ($AV^-$, $PI^-$, lower left quadrant) in percentage of total gated cells. One representative experiment of three similar repeats is shown. PARP-1 knockdown was confirmed by expression analysis using immunoblot detection (bottom panel) as specified in Materials and methods.

(3-ABA) and PJ34 known to antagonize PARP-dependent ATP depletion in response to genotoxic stress (Figure 5B) [35]. Next, we tested the possibility that genetic antagonism of PARP-1 expression using siRNA may suppress DCPIP-induced cell death (Figure 5C). Again, MDA-MB231 cells with strongly attenuated PARP-1 protein levels (siPARP-1) as confirmed by immunoblot detection (Figure 5C, lower panel) were not protected from DCPIP-induced loss of viability. Follow-up experimentation aiming at immunoblot detection of poly(ADP-ribose) polymers in cellular protein extracts prepared from DCPIP-treated cells at early time points (15 min–3 h) remained unsuccessful (data not shown). Taken together, these data exclude a mechanistic involvement of DNA-damage-dependent PARP-1 activation in early ATP depletion (Figure 3B) or caspase-independent MDA-MB231 cell death that occurs in response to DCPIP treatment (Figures 1A–C).

### *Intraperitoneal administration of DCPIP impairs growth of MDA-MB231 human breast carcinoma xenografts in SCID mice*

Based on the low acute and chronic systemic toxicity of DCPIP as documented earlier in mice [24], combined with the significant DCPIP-sensitivity of MDA-MB231 cells displaying the homozygous NQO1*2 genotype, we tested DCPIP as a potential inhibitor of tumour growth in a human MDC-MB231 breast carcinoma SCID-mouse xenograft model (Figure 6).

Daily intraperitoneal DCPIP treatment (10 mg × $kg^{-1}$ × $d^{-1}$) of human MDA-MB231 xenograft-bearing SCID mice induced a significant suppression of tumour growth that reached the level of statistical

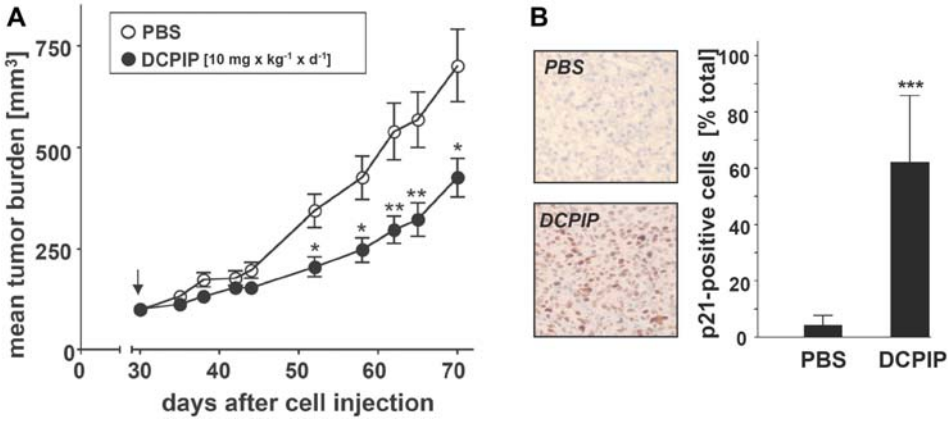


Figure 6. DCPIP impairs homozygous NQO1*2 tumour growth in a human MDA-MB231 breast carcinoma SCID-mouse xenograft model. Human MDA-MB231 breast carcinoma cells ($10 \times 10^6$) in matrigel were injected into the mammary fat pad of female SCID mice; 30 days after cell injection animals were pair-matched (65 $mm^3$ average tumour size) and 1 day later (vertical arrow) daily treatment (DCPIP: 10 mg $\times$ $kg^{-1} \times d^{-1}$, 100 µl, b.i.d., $n = 10$; control group: PBS only, 100 µl, b.i.d., $n = 12$) was initiated by intraperitoneal injection as specified in Materials and methods. (A) Tumour growth curves were obtained by determining average tumour volumes until day 70 after cell injection. Data points are depicted as means ± SEM and statistical comparison between individual data points was performed using the two-sided Student's *t*-test ($^{*}p < 0.05$; $^{**}p < 0.01$; $^{***}p < 0.001$). (B) Immunohistochemical staining for p21 using primary tumour tissue of DCPIP-treated and PBS-treated mice sacrificed on day 70 ($n = 3$, each group). Paraformaldehyde-fixed, paraffin-embedded 5 µm sections were analysed using a mouse monoclonal antibody to p21 followed by biotinylated-streptavidin-HRP/DAB visualization. Haematoxylin counterstaining was also performed. A photograph representative of three high power fields taken per tissue section is shown, displaying the cortical rim region of the tumours. Bar graph displays quantitative analysis of p21 IHC (percentage p21 positive cells per high power field; mean ± SD; $n = 3$).



significance ($p < 0.05$; DCPIP- vs PBS-treated control) between days 52 and 70 after cell injection, where average tumour volumes of DCPIP-treated animals were up to 42% lower than that of PBS-treated controls (Figure 6A; day 52). Indicative of a significant attenuation of tumour cell proliferation by DCPIP, immunohistochemical detection revealed significant up-regulation of p21 protein-epitope expression in tumours of DCPIP-treated animals (Figure 6B), a result consistent with DCPIP-induced up-regulation of CDKN1A gene expression on the transcriptional and protein level as observed in cell culture experiments (Figures 2A, E and F).

## Discussion

Breast cancer is the second most common type of non-skin cancer worldwide, surpassed in incidence only by lung cancer. In the US alone, more than 40 000 women die each year from metastatic breast cancer and an urgent need for novel treatment modalities and improved molecular therapeutics exists [48]. Importantly, recent progress in personalized medicine has significantly impacted the preventative and therapeutic care directed towards breast cancer where treatment of tumour sub-types is guided by receptor expression status that includes the oestrogen-, progesterone- and her2/neu-receptors [49–51]. Genetic testing for disease-causing mutations in the tumour suppressor genes *BRCA1* (breast cancer type 1 susceptibility protein) and *BRCA2* can identify individuals at risk of familial breast cancer and may enable synthetic lethal chemotherapy employing PARP-1 inhibitors [49,52]. Targeted molecular therapy using the monoclonal antibody trastuzumab has shown clinical efficacy in HER2/neu (Human Epidermal growth factor Receptor 2) positive breast cancer where HER2 over-expression is associated with increased aggressiveness and more frequent disease recurrence [50,51].

Here, we present novel experimental evidence suggesting that the homozygous NQO1*2 genotype, present with up to 20% frequency in human breast cancer patients [29,31], may be associated with a specific chemical vulnerability of breast carcinoma cells that can be targeted by chemotherapeutic intervention. Extensive drug development has aimed at developing bioreductively-activated chemotherapeutics including mitomycin C, the indoloquinone E09, beta-lapachone and phenothiazinium-based redox cyclers, all of which undergo NQO1-dependent activation with induction of cytotoxic oxidative and/or alkylating stress targeting tumour types that display NQO1 over-expression [28,30,32,47,53]. In contrast, no progress has been achieved in designing experimental chemotherapeutics that are directed against NQO1-deficient tumours including homozygous NQO1*2 breast carcinoma. Based on earlier research that has demonstrated the anti-melanoma activity of the experimental redox chemotherapeutic DCPIP that is antagonized by cellular NQO1 expression [24], we now present data that indicate feasibility of targeting experimental homozygous NQO1*2 breast carcinoma using DCPIP *in vitro* and *in vivo*.

Indeed, systemic administration of DCPIP displayed significant activity in the MDA-MB231 murine xenograft model of human homozygous NQO1*2 breast adenocarcinoma. Daily intraperitoneal administration of DCPIP (10 mg $\times$ $kg^{-1}$ $\times$ $d^{-1}$) resulted in a significant suppression of tumour growth (Figure 6A) that was accompanied by up-regulation of p21 protein levels in tumour tissue of DCPIP-treated animals (Figure 6B). However, the dose–response relationship of DCPIP anti-tumour activity was not further explored in this limited prototype study. Moreover, due to the intrinsic limitations associated with the current xenograft model that is based on treating human NQO1*2 MDA-MB231 tumours implanted into NQO1 wild-type mice, the therapeutic window of DCPIP-chemotherapeutic intervention remains largely undefined. Future experimentation using improved xenograft models with more predictive value will aim at addressing the important question if specificity of DCPIP cytotoxicity directed towards NQO1*2 breast carcinoma cells is maintained in a host organism that displays the NQO1*2 genotype. Nevertheless, the absence of DCPIP-associated systemic or organ toxicity observed earlier in an A375 melanoma murine xenograft model suggests feasibility of DCPIP-based anti-cancer intervention without causing collateral damage to normal murine tissues that may display low expression levels of endogenous NQO1 including liver and kidney [24,54]. In complimentary cell culture experiments, we observed that DCPIP treatment caused caspase-independent cell death in human MDA-MB231 breast carcinoma cells displaying the homozygous NQO1*2 genotype. In contrast to MDA-MB231 cells displaying DCPIP-hypersensitivity (Figures 1A–C and E), MCF7 breast carcinoma cells over-expressing NQO1 (MCF7-DT15) or MCF7 control transfectants (MCF7-neo2) expressing appreciable endogenous levels of NQO1 were largely resistant to DCPIP-induced glutathione depletion and cytotoxicity (Figures 1D and E and 4A).

In MDA-MB231 cells, DCPIP rapidly induced oxidative and genotoxic stress associated with impaired genomic integrity and glutathione depletion that were detectable within 30 min exposure (Figures 2–5). DCPIP also induced early mitochondrial dysfunction (Figure 3C) and energy crisis (Figure 3B) observable at time points before viability was compromised (Figure 4B), suggesting that these rapid functional changes are causatively involved in cell death induction and are not mere epiphenomena of necrotic cell disintegration and plasma membrane permeabilization.

It has been shown earlier that PARP-1 activation in response to drug-induced genotoxic stress may lead to rapid depletion of the cellular $NAD^+$ and ATP pools initiating a PARP-dependent yet caspase-independent mode of cell death as observed with the NQO1-dependent redox chemotherapeutic beta-lapachone, a pro-oxidant quinone targeting non-small cell lung carcinoma cells [47]. However, a mechanistic role of early PARP-1 activation in the causation of DCPIP-induced energy crisis was ruled out by demonstrating that pharmacological or genetic PARP-1 antagonism did not suppress DCPIP-induced ATP depletion or cytotoxicity. It is therefore more likely that DCPIP-induced ATP depletion (detectable at 6 h exposure; Figure 3B) occurred as a result of mitochondrial impairment, as obvious from loss of mitochondrial membrane potential (detectable at 3 h; Figure 3C) after glutathione depletion (detectable at 30 min; Figure 4A), up-regulation of cellular peroxide levels (detectable at 1 h; Figure 3A) and early impairment of genomic integrity (detectable at 30 min; Figure 5A). Loss of viability downstream of this molecular sequence is compatible with a caspase-independent mode of MDA-MB231 cell death (as observed in Figures 1A–C) where cell death occurs without activation of the executioner caspase 3 and cannot be blocked by pharmacological pancaspase inhibition. Earlier research has shown that DCPIP can induce apoptosis in cultured human A375 and G361 melanoma cells, but these cells display at least moderate NQO1 specific enzymatic activity (A375: 280 $\pm$ 40; G361: 2400 $\pm$ 220 (nmol reduced DCPIP $\times$ (mg cellular protein)$^{-1}$ $\times$ $min^{-1}$) as published earlier [32]) that would attenuate DCPIP cytotoxicity to an extent that programmed apoptotic cell death can still be executed. In contrast, rapid depletion of cellular ATP and glutathione together with early up-regulation of a massive heat shock response (Hsp70 and Hsp70B'; Figures 2A–D), known to block initiation and energy-dependent execution of apoptotic cell death [55], may explain the different cell death mode observed in DCPIP-hypersensitive MDA-MB231 characterized by complete absence of NQO1 specific enzymatic activity.

Consistent with pronounced induction of cellular stress, up-regulated expression of established oxidative (GSTM3, HMOX1 and EGR1), heat shock (HSPA6, HSPA1A, HMOX1 and CRYAB) and genotoxic stress response (GADD45A, CDKN1A) genes was detected by detailed array analysis of MDA-MB231 cells exposed to DCPIP (Figure 2A). DCPIP-induced up-regulation of gene expression was then examined by Western-analysis of HO-1, Hsp70, Hsp70B' and p21 protein levels (Figures 2B–G). Early activational phosphorylation of p53 [phospho-p53 (Ser 15)] and up-regulation of p21 protein levels occurred within 3 h exposure to DCPIP, consistent with the early onset of a genotoxic stress response as detected by the comet assay (Figure 5A) [56]. However, the molecular mechanism underlying DCPIP genotoxicity and p21 up-regulation and its causative relationship to early depletion of glutathione and induction of oxidative stress remains unresolved at this point and awaits further experimentation [42]. Importantly, DCPIP-induced up-regulation of p21 cellular protein levels was also observed upon immunohistochemical analysis of MDA-MB231 xenograft tumours harvested from DCPIP-treated SCID mice, suggesting

that p21 target modulation by DCPIP may be achieved *in vivo* (Figure 6B).

Numerous pro-oxidant quinone-derivatives display anti-cancer activity that is thought to involve ROS formation via redox cycling and thiol-adduction of protein- and glutathione-cysteine residues [36,57–59]. Moreover, earlier experimentation involving isolated mitochondria has indicated that DCPIP can serve as an artificial electron acceptor from the respiratory chain, also serving as an artificial substrate (Hill reagent) for chloroplast-mediated photoreduction [60–62]. Our data describing the effects of oxygen availability on DCPIP-associated anti-cancer activity indicate that DCPIP-induced cytotoxicity and early depletion of cellular glutathione are equally pronounced under normoxic as well as hypoxic conditions (Figure 4E). Experiments examining mitochondrial integrity, based on flow cytometric assessment of transmembrane potential (Figure 3C), suggest that glutathione depletion and cellular oxidative stress precede loss of mitochondrial function, positioning a potential mitochondrial impairment by DCPIP downstream of earlier events that affect the cellular glutathione pool.

Additional chemical redox experimentation using an oxygen electrode indicated that DCPIP does not undergo ascorbate-driven redox cycling, potentially leading to reductive oxygen depletion (Figure 4F), an activity well documented for the quinone-type pro-oxidant menadione [36]. This differential redox reactivity may be related to the more positive redox potential of DCPIP vs menadione ($E'^{o}$ (menadione) = +0.14 V) and is also consistent with the established use of DCPIP as a photometric reagent for stochiometric redox titration of ascorbate, an analytical use that would be incompatible with redox cycling of DCPIP [63].

Our limited structure–activity relationship study involving the dehalogenated DCPIP-analogue phenolindophenol [PIP, 4-(4-hydroxyphenyl)-iminocyclohexa-2,5-dien-1-one] demonstrated that the absence of the two chlorine atoms from the 2- and 6-positions of the aromatic quinoneimine core completely abolished cytotoxic and glutathione-depleting activity of the test compound (Figures 4G and H), suggesting a crucial role of these electronegative substituents in thiol-directed electrophilic activation and chemotherapeutic activity of DCPIP. Further analysis revealed that DCPIP-induced depletion of cellular reduced glutathione was not a result of glutathione oxidation to the disulphide form (either as the glutathione dimer or protein-bound mixed disulphides), since reductive pretreatment using TCEP (*tris*(2-carboxyethyl) phosphine; as specified in Material and methods) did not recover appreciable levels of reduced glutathione in our luminescence-based homogeneous assay performed on total cells (data not shown). Moreover, extracellular glutathione levels remained at an undetectable level (data not shown) and membrane integrity was undisturbed at time points at which massive DCPIP-induced glutathione depletion was detectable (Figures 4A and B), excluding an involvement of impaired membrane integrity or cellular export in intracellular glutathione depletion. In contrast, preliminary mass spectrometric analysis indicated rapid formation of DCPIP-glutathione conjugates that may form through Michael addition and nucleophilic substitution reactions at the chlorine substituents, known to be involved in quinone-thiol conjugation reactions (data not shown) [45,64,65]. These data are compatible with earlier chemical experimentation that has demonstrated the rapid formation of mono- and disubstituted S-glutathionyl-2,6-dichlorophenolindophenols between DCPIP and glutathione under conditions of physiological temperature and pH [44]. Current follow-up experimentation in live cells aims at substantiating covalent adduction of DCPIP by glutathione as the crucial molecular mechanism underlying rapid loss of intracellular glutathione observed in MDA-MB231 cells. It is also interesting to note that early biochemical research has documented the ability of DCPIP to covalently react with protein-bound thiol groups, suggesting the possibility that DCPIP cytotoxicity may result in part from thioalkylation of crucial protein-bound cysteine target residues, a possibility to be explored by future experiments [66].

Taken together, the findings presented in this study strongly suggest that the absence of enzymatically active NQO1 may be the molecular factor that determines the specific chemical vulnerability of homozygous NQO1*2 MDA-MB231 breast carcinoma cells towards DCPIP-induced cytotoxicity. Earlier research indicates that pharmacological induction of oxidative stress through modulation of redox sensitive targets may provide therapeutic benefit in the context of tumour chemosensitization and chemotherapy [3,4]. Future experiments will further explore molecular mechanism and therapeutic potential of the pro-oxidant DCPIP as a combinatorial or stand-alone genotype-directed experimental chemotherapeutic targeting NQO1*2 breast carcinoma and other tumours characterized by a redox vulnerability originating from NQO1 deficiency.

## Acknowledgements

Supported in part by grants from the National Institutes of Health [R01CA122484, ES007091, ES06694, Arizona Cancer Center Support Grant CA023074]. Animal experimentation was performed at the AZCC experimental mouse shared service (EMSS). 'CMC was supported by a pre-doctoral fellowship from the American Chemical Society, Division of Medicinal Chemistry sponsored by Novartis.

## Declaration of interest

The authors report no conflicts of interest. The content is solely the responsibility of the authors and does not necessarily represent the official views of the National Cancer Institute or the National Institutes of Health.

## References


[1] Fruehauf JP, Meyskens FL, Jr. Reactive oxygen species: a breath of life or death? Clin Cancer Res 2007;13:789–794.

[2] Cabello CM, Bair WB, III, Wondrak GT. Experimental therapeutics: targeting the redox Achilles heel of cancer. Curr Opin Investig Drugs 2007;8:1022–1037.

[3] Trachootham D, Alexandre J, Huang P. Targeting cancer cells by ROS-mediated mechanisms: a radical therapeutic approach? Nat Rev Drug Discov 2009;8:579–591.

[4] Wondrak GT. Redox-directed cancer therapeutics: molecular mechanisms and opportunities. Antioxid Redox Signal 2009; 11:3013–3069.

[5] Trachootham D, Lu W, Ogasawara MA, Nilsa RD, Huang P. Redox regulation of cell survival. Antioxid Redox Signal 2008; 10:1343–1374.

[6] Liou GY, Storz P. Reactive oxygen species in cancer. Free Radic Res 2010;44:479–496.

[7] Fry FH, Holme AL, Giles NM, Giles GI, Collins C, Holt K, Pariagh S, Gelbrich T, Hursthouse MB, Gutowski NJ, Jacob C. Multifunctional redox catalysts as selective enhancers of oxidative stress. Org Biomol Chem 2005;3:2579–2587.

[8] Schumacker PT. Reactive oxygen species in cancer cells: live by the sword, die by the sword. Cancer Cell 2006;10: 175–176.

[9] Zhang H, Trachootham D, Lu W, Carew J, Giles FJ, Keating MJ, Arlinghaus RB, Huang P. Effective killing of Gleevec-resistant CML cells with T315I mutation by a natural compound PEITC through redox-mediated mechanism. Leukemia 2008;22:1191–1199.

[10] Verrax J, Pedrosa RC, Beck R, Dejeans N, Taper H, Calderon PB. *In situ* modulation of oxidative stress: a novel and efficient strategy to kill cancer cells. Curr Med Chem 2009;16: 1821–1830.

[11] Beck R, Pedrosa RC, Dejeans N, Glorieux C, Leveque P, Gallez B, Taper H, Eeckhoudt S, Knoops L, Calderon PB, Verrax J. Ascorbate/menadione-induced oxidative stress kills cancer cells that express normal or mutated forms of the oncogenic protein Bcr-Abl. An *in vitro* and *in vivo* mechanistic study. Invest New Drugs 2010; May 8 [Epub ahead of print] DOI: 10.1007/s10637-010-9441-3.

[12] Moehler TM, Feneberg R, Ho AD, Golenkov AK, Ludwig H, Kropff M, Khuageva NK, Hajda J, von Broen I, Goldschmidt H. Combined phase I/II study of imexon (AOP99.0001) for treatment of relapsed or refractory multiple myeloma. Anticancer Drugs 2010;21:708–715.

[13] Saulnier Sholler GL, Brard L, Straub JA, Dorf L, Illeyne S, Koto K, Kalkunte S, Bosenberg M, Ashikaga T, Nishi R. Nifurtimox induces apoptosis of neuroblastoma cells *in vitro* and *in vivo*. J Pediatr Hematol Oncol 2009;31:187–193.

[14] Efferth T. Molecular pharmacology and pharmacogenomics of artemisinin and its derivatives in cancer cells. Curr Drug Targets 2006;7:407–421.

[15] Berger TG, Dieckmann D, Efferth T, Schultz ES, Funk JO, Baur A, Schuler G. Artesunate in the treatment of metastatic uveal melanoma–first experiences. Oncol Rep 2005;14:599–1603.

[16] Lin TS, Naumovski L, Lecane PS, Lucas MS, Moran ME, Cheney C, Lucas DM, Phan SC, Miller RA, Byrd JC. Effects of motexafin gadolinium in a phase II trial in refractory chronic lymphocytic leukemia. Leuk Lymphoma 2009;50:1977–1982.

[17] Donate F, Juarez JC, Burnett ME, Manuia MM, Guan X, Shaw DE, Smith EL, Timucin C, Braunstein MJ, Batuman OA, Mazar AP. Identification of biomarkers for the antiangiogenic and antitumour activity of the superoxide dismutase 1 (SOD1) inhibitor tetrathiomolybdate (ATN-224). Br J Cancer 2008;98:776–783.

[18] Mann KK, Wallner B, Lossos IS, Miller WH, Jr. Darinaparsin: a novel organic arsenical with promising anticancer activity. Expert Opin Investig Drugs 2009;18:1727–1734.

[19] Ramanathan RK, Abbruzzese J, Dragovich T, Kirkpatrick L, Guillen JM, Baker AF, Pestano LA, Green S, Von Hoff DD. A randomized phase II study of PX-12, an inhibitor of thioredoxin in patients with advanced cancer of the pancreas following progression after a gemcitabine-containing combination. Cancer Chemother Pharmacol 2010; May 12 [Epub ahead of print] DOI: 10.1007/s00280-010-1343-8.

[20] Chen Y, Jungsuwadee P, Vore M, Butterfield DA, St Clair DK. Collateral damage in cancer chemotherapy: oxidative stress in nontargeted tissues. Mol Interv 2007;7:147–156.

[21] Ramanathan B, Jan KY, Chen CH, Hour TC, Yu HJ, Pu YS. Resistance to paclitaxel is proportional to cellular total antioxidant capacity. Cancer Res 2005;65:8455–8460.

[22] Baker AF, Dragovich T, Tate WR, Ramanathan RK, Roe D, Hsu CH, Kirkpatrick DL, Powis G. The antitumor thioredoxin-1 inhibitor PX-12 (1-methylpropyl 2-imidazolyl disulfide) decreases thioredoxin-1 and VEGF levels in cancer patient plasma. J Lab Clin Med 2006;147:83–90.

[23] Singh A, Misra V, Thimmulappa RK, Lee H, Ames S, Hoque MO, Herman JG, Baylin SB, Sidransky D, Gabrielson E, Brock MV, Biswal S. Dysfunctional KEAP1-NRF2 interaction in non-small-cell lung cancer. PLoS Med 2006;3:e420.

[24] Cabello CM, Bair WB, III, Bause AS, Wondrak GT. Antimelanoma activity of the redox dye DCPIP (2,6-dichlorophenolindophenol) is antagonized by NQO1. Biochem Pharmacol 2009;78:344–354.

[25] MSDS. 2,6-dichlorophenolindophenol sodium salt (CAS#620-45-1). Sigma-Aldrich 2006; Version 1.5, 01/31/2006.

[26] Mondalek FG, Ponnurangam S, Govind J, Houchen C, Anant S, Pantazis P, Ramanujam RP. Inhibition of angiogenesis- and inflammation-inducing factors in human colon cancer cells *in vitro* and *in ovo* by free and nanoparticle-encapsulated redox dye, DCPIP. J Nanobiotechnology 2010;8:17.

[27] Siegel D, Anwar A, Winski SL, Kepa JK, Zolman KL, Ross D. Rapid polyubiquitination and proteasomal degradation of a mutant form of NAD(P)H:quinone oxidoreductase 1. Mol Pharmacol 2001;59:263–268.

[28] Ross D, Siegel D. NAD(P)H:quinone oxidoreductase 1 (NQO1, DT-diaphorase), functions and pharmacogenetics. Meth Enzymol 2004;382:115–144.

[29] Fagerholm R, Hofstetter B, Tommiska J, Aaltonen K, Vrtel R, Syrjakoski K, Kallioniemi A, Kilpivaara O, Mannermaa A, Kosma VM, Uusitupa M, Eskelinen M, Kataja V, Aittomaki K, von Smitten K, Heikkila P, Lukas J, Holli K, Bartkova J, Blomqvist C, Bartek J, Nevanlinna H. NAD(P)H:quinone oxidoreductase 1 NQO1*2 genotype (P187S) is a strong prognostic and predictive factor in breast cancer. Nat Genet 2008; 40:844–853.

[30] Siemankowski LM, Morreale J, Butts BD, Briehl MM. Increased tumor necrosis factor-alpha sensitivity of MCF-7 cells transfected with NAD(P)H:quinone reductase. Cancer Res 2000;60:3638–3644.

[31] Menzel HJ, Sarmanova J, Soucek P, Berberich R, Grunewald K, Haun M, Kraft HG. Association of NQO1 polymorphism with spontaneous breast cancer in two independent populations. Br J Cancer 2004;90:1989–1994.

[32] Wondrak GT. NQO1-activated phenothiazinium redox cyclers for the targeted bioreductive induction of cancer cell apoptosis. Free Radic Biol Med 2007;43:178–190.

[33] Cabello CM, Bair WB, III, Ley S, Lamore SD, Azimian S, Wondrak GT. The experimental chemotherapeutic N(6)-furfuryladenosine (kinetin-riboside) induces rapid ATP depletion, genotoxic stress, and CDKN1A (p21) upregulation in human cancer cell lines. Biochem Pharmacol 2009;77: 1125–1138.

[34] Cabello CM, Bair WB, III, Lamore SD, Ley S, Bause AS, Azimian S, Wondrak GT. The cinnamon-derived Michael

acceptor cinnamic aldehyde impairs melanoma cell proliferation, invasiveness, and tumor growth. Free Radic Biol Med 2009;46:220–231.
[35] Lamore SD, Cabello CM, Wondrak GT. The topical antimicrobial zinc pyrithione is a heat shock response inducer that causes DNA damage and PARP-dependent energy crisis in human skin cells. Cell Stress Chaperones 2010;15:309–322.
[36] Verrax J, Delvaux M, Beghein N, Taper H, Gallez B, Buc Calderon P. Enhancement of quinone redox cycling by ascorbate induces a caspase-3 independent cell death in human leukaemia cells. An *in vitro* comparative study. Free Radic Res 2005;39:649–657.
[37] Wondrak GT, Jacobson MK, Jacobson EL. Antimelanoma activity of apoptogenic carbonyl scavengers. J Pharmacol Exp Ther 2006;316:805–814.
[38] Noonan E, Giardina C, Hightower L. Hsp70B' and Hsp72 form a complex in stressed human colon cells and each contributes to cytoprotection. Exp Cell Res 2008;314:468–2476.
[39] Baron V, Adamson ED, Calogero A, Ragona G, Mercola D. The transcription factor Egr1 is a direct regulator of multiple tumor suppressors including TGFbeta1, PTEN, p53, and fibronectin. Cancer Gene Ther 2006;13:115–124.
[40] Sarkar D, Su ZZ, Lebedeva IV, Sauane M, Gopalkrishnan RV, Valerie K, Dent P, Fisher PB. mda-7 (IL-24) mediates selective apoptosis in human melanoma cells by inducing the coordinated overexpression of the GADD family of genes by means of p38 MAPK. Proc Natl Acad Sci USA 2002;99: 10054–10059.
[41] Scott DW, Loo G. Curcumin-induced GADD153 gene up-regulation in human colon cancer cells. Carcinogenesis 2004; 25:2155–2164.
[42] O'Reilly MA. Redox activation of p21Cip1/WAF1/Sdi1: a multifunctional regulator of cell survival and death. Antioxid Redox Signal 2005;7:108–118.
[43] Rong JJ, Hu R, Song XM, Ha J, Lu N, Qi Q, Tao L, You QD, Guo QL. Gambogic acid triggers DNA damage signaling that induces p53/p21(Waf1/CIP1) activation through the ATR-Chk1 pathway. Cancer Lett 2010;296:55–64.
[44] Coffey DS, Hellerman L. Oxidation of biological thiols: glutathione-indophenol interactions. Biochemistry 1964;3: 394–402.
[45] Song Y, Buettner GR. Thermodynamic and kinetic considerations for the reaction of semiquinone radicals to form superoxide and hydrogen peroxide. Free Radic Biol Med 2010;49: 919–962.
[46] Tice RR, Agurell E, Anderson D, Burlinson B, Hartmann A, Kobayashi H, Miyamae Y, Rojas E, Ryu JC, Sasaki YF. Single cell gel/comet assay: guidelines for *in vitro* and *in vivo* genetic toxicology testing. Environ Mol Mutagen 2000;35:206–221.
[47] Bey EA, Bentle MS, Reinicke KE, Dong Y, Yang CR, Girard L, Minna JD, Bornmann WG, Gao J, Boothman DA. An NQO1- and PARP-1-mediated cell death pathway induced in non-small-cell lung cancer cells by beta-lapachone. Proc Natl Acad Sci USA 2007;104:11832–11837.
[48] Anders CK, Carey LA. Biology, metastatic patterns, and treatment of patients with triple-negative breast cancer. Clin Breast Cancer 2009;9(Suppl 2):73–81.
[49] Gulati AP, Domchek SM. The clinical management of BRCA1 and BRCA2 mutation carriers. Curr Oncol Rep 2008;10:47–53.
[50] Murphy CG, Fornier M. HER2-positive breast cancer: beyond trastuzumab. Oncology (Williston Park) 2010;24:410–415.
[51] Longo R, D'Andrea M, Sarmiento R, Gasparini G. Pharmacogenetics in breast cancer: focus on hormone therapy, taxanes, trastuzumab and bevacizumab. Expert Opin Investig Drugs 2010;19(Suppl 1):41–50.
[52] Fong PC, Boss DS, Yap TA, Tutt A, Wu P, Mergui-Roelvink M, Mortimer P, Swaisland H, Lau A, O'Connor MJ, Ashworth A, Carmichael J, Kaye SB, Schellens JH, de Bono JS. Inhibition of poly(ADP-ribose) polymerase in tumors from BRCA mutation carriers. N Engl J Med 2009;361:123–134.
[53] Wang XJ, Sun Z, Villeneuve NF, Zhang S, Zhao F, Li Y, Chen W, Yi X, Zheng W, Wondrak GT, Wong PK, Zhang DD. Nrf2 enhances resistance of cancer cells to chemotherapeutic drugs, the dark side of Nrf2. Carcinogenesis 2008;29: 1235–1243.
[54] de Haan LH, Pot GK, Aarts JM, Rietjens IM, Alink GM. *In vivo* relevance of two critical levels for NAD(P)H:quinone oxidoreductase (NQO1)-mediated cellular protection against electrophile toxicity found *in vitro*. Toxicol *In Vitro* 2006;20: 594–600.
[55] Lanneau D, Brunet M, Frisan E, Solary E, Fontenay M, Garrido C. Heat shock proteins: essential proteins for apoptosis regulation. J Cell Mol Med 2008;12:743–761.
[56] Weiss RH. p21Waf1/Cip1 as a therapeutic target in breast and other cancers. Cancer Cell 2003;4:425–429.
[57] Abdelmohsen K, Gerber PA, von Montfort C, Sies H, Klotz LO. Epidermal growth factor receptor is a common mediator of quinone-induced signaling leading to phosphorylation of connexin-43: role of glutathione and tyrosine phosphatases. J Biol Chem 2003;278:38360–38367.
[58] Schmieder PK, Tapper MA, Kolanczyk RC, Hammermeister DE, Sheedy BR, Denny JS. Discriminating redox cycling and arylation pathways of reactive chemical toxicity in trout hepatocytes. Toxicol Sci 2003;72:66–76.
[59] Verrax J, Taper H, Buc Calderon P. Targeting cancer cells by an oxidant-based therapy. Curr Mol Pharmacol 2008;1:80–92.
[60] Yamashita T, Butler WL. Photoreduction and photophosphorylation with tris-washed chloroplasts. Plant Physiol 1968;43: 1978–1986.
[61] Mayer D, Naumann R, Edler L, Bannasch P. Investigation by amperometric methods of intracellular reduction of 2,6-dichlorophenolindophenol in normal and transformed hepatocytes in the presence of different inhibitors of cellular metabolism. Biochim Biophys Acta 1990;1015:258–263.
[62] Kumar S, Acharya SK. 2,6-Dichloro-phenol indophenol prevents switch-over of electrons between the cyanide-sensitive and -insensitive pathway of the mitochondrial electron transport chain in the presence of inhibitors. Anal Biochem 1999; 268:89–93.
[63] VanderJagt DJ, Garry PJ, Hunt WC. Ascorbate in plasma as measured by liquid chromatography and by dichlorophenolindophenol colorimetry. Clin Chem 1986;32:1004–1006.
[64] Song Y, Wagner BA, Witmer JR, Lehmler HJ, Buettner GR. Nonenzymatic displacement of chlorine and formation of free radicals upon the reaction of glutathione with PCB quinones. Proc Natl Acad Sci USA 2009;106:9725–9730.
[65] Lau SS, Hill BA, Highet RJ, Monks TJ. Sequential oxidation and glutathione addition to 1,4-benzoquinone: correlation of toxicity with increased glutathione substitution. Mol Pharmacol 1988;34:829–836.
[66] Coffey DS, Hellerman L. The interaction of 2,6-dichloroindophenol and protein sulfhydryl groups. Biochim Biophys Acta 1965;100:98–103.

This paper was first published online on Early Online on 25 October 2010.